Mathematical modelling of how wave breaking might be imaged by a radar.

Peter James Nee

26-07-21

Contents

1 Introduction

The description and identification of wave breaking is a complicated issue with ongoing research being performed. With no standard definition, it is usually described as the conversion of wave energy into other forms of energy (heat, optical, sound, turbulence) [7]. The scale of breaking events may vary, both temporally and spatially. The signature of wave breaking can be detected through a variety of means.

One of the most common and useful methods for imaging sea surfaces is radar imaging [2]. In combination with optical data, it can be particularly useful in the prediction, detection and measurement of wave breaking. One can use this data to properly discern between breaking events, steepened non-breaking waves, and remnant foam, as well as collect a range of information about the sea state.

The type of breaking present relies greatly on the depth of the water and bathymetry that is present. In deep-water oceans one often observes non-linear effects leading to extreme wave heights, also known as "swelling". In surf-zone and near-shore currents, one has to account for shoaling: the process by which as a wave train approaches the shore/enters shallower depths, there is often an increase in amplitude and decrease in wave length. One such set of conditions comes from linear wave theory, which can be derived from the mild slope equations [3].

2 Sea Surface Simulations under Shoaling Conditions

The 1D sea surface for linear shoaling conditions, as a function of space and time, is given by:

$$\zeta\left(x,t\right)=\Re\left(\sum_{j=1}^{N}a_{j}\left(x\right)e^{i\left(\omega_{j}t-\int_{0}^{x}k_{j}(\xi)d\xi+\phi_{j}\right)}\right), \tag{1}$$

where a_j is the amplitude of the wave component corresponding to an angular frequency of ω_j and wave number k_j, that is uniformly distributed over $[0, 2\pi)$ initial phase ϕ_j. The constraint placed upon these angular frequencies and wave numbers is the dispersion relation:

$$\omega_{j}^{2}=gk_{j}\left(x\right)\tanh\left(k_{j}(x)h(x)\right), \tag{2}$$

where g is the gravitational constant, and $h(x)$ is a function which describes the bathymetry.

Moving onto the linear shoaling of the sea state, this process is described by the one dimensional mild slope equation [3]:

$$\frac{a_{j}'(x)}{a_{j}(x)}=-\frac{C_{g,j}'(x)}{2C_{g,j}(x)}, \tag{3}$$

where $C_{g,j}$ is the corresponding group velocity, defined as:

$$C_{g,j}(x)=\frac{\omega_{j}}{2k_{j}(x)}\left(1+\frac{2k_{j}(x)h(x)}{\sinh(2k_{j}(x)h(x))}\right). \tag{4}$$

This mild slope equation can then be rewritten as:

$$\frac{\mathrm{d}}{\mathrm{dx}}\left(\ln\left(a_{j}(x)\right)\right)=-\frac{1}{2}\frac{\mathrm{d}}{\mathrm{dx}}\left(\ln\left(C_{g,j}(x)\right)\right). \tag{5}$$

Bringing the half inside the differential and integrating yields the equation:

$$a_{j}(x)=a_{j}(0)\sqrt{\frac{C_{g,j}(0)}{C_{g,j}(x)}}. \tag{6}$$

We present two cases for $a_j(0)$: a simple monochromatic wave ($a_j(0) = 1$, and a JONSWAP spectra ($a_j(0) = \sqrt{2\int_{w_j-\frac{1}{2}\Delta\omega}^{w_j+\frac{1}{2}\Delta\omega}S(\omega)d\omega}$). In the latter case, the spectra $S(\omega)$ is calculated via:

$$S_{j}(\omega)=\frac{g^{2}\alpha}{\omega^{5}}\exp\left[-\frac{5}{4}\left(\frac{\omega_{p}}{\omega}\right)^{4}\right]\gamma^{r}, \tag{7}$$

where:

$$r=\exp\left[-\frac{(\omega-\omega_{p})^{2}}{2\sigma^{2}\omega_{p}^{2}}\right], \tag{8}$$

with the remaining constants given in the table below.

Table 1: List of parameters used in shoaling simulations.

α	$0.076\left(\frac{U_{10}^{2}}{Fg}\right)^{0.22}$, where $F = 300000$
ω_p	$1/Tp$, where $Tp = 12$
γ	3.3
σ	0.07 if $\omega \leq \omega$, 0.09 otherwise
g	9.8

For the purpose of this demonstration, we have used a simple bathymetry of a depth that increases linearly away from the shore, with two plateaus either side. The analytic expression is given by:

$$h(x) = \begin{cases} -10 & x \leq 700 \\ -0.05x + 25 & 700 \leq x \leq 1700 \\ -60 & 1700 \leq x, \end{cases}$$

Evaluating our sea state at $t_0 = 0$, we obtain the following plots:

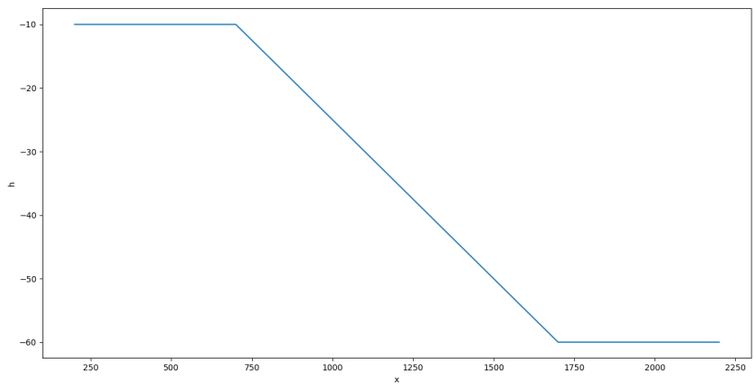

Figure 1: Simple bathymetry used for shoaling simulations.

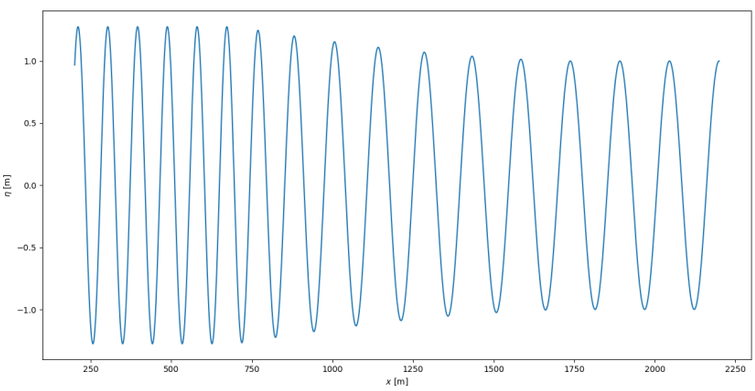

Figure 2: Simulation of a sinusoidal wave under shoaling conditions.

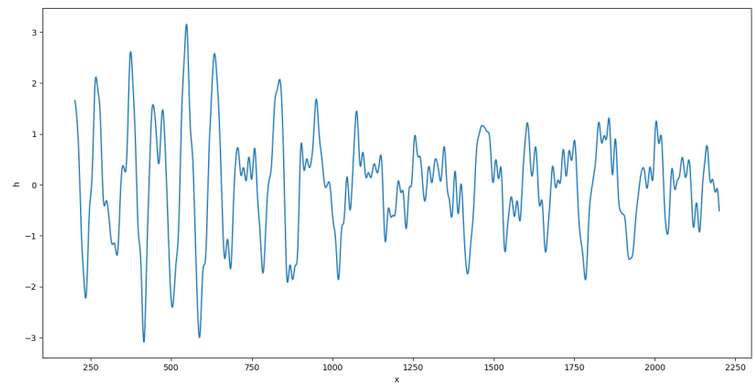

Figure 3: Simulation of a JONSWAP spectra under shoaling conditions.

In both cases, an increase in wave amplitude and decrease in wavelength is clearly visible closer to the shore. This is very much in line with experimental observations.

3 Breaking Detection of 1D Simulated Sea Surfaces

Given the simulations in the previous section, we wanted to devise an algorithm that would effectively find and track the different peaks that occur, and apply some form of breaking criterion to these peaks to distinguish

between large waves and breaking ones. First, we wrote an algorithm that tracks each individual peak in the data, and calculates the crest and particle speed at that point. The peaks are defined as maximums between zero crossings, and are tracked through time and space.

As the precise reasons for wave breaking are still an area of ongoing research, there is no absolute way to determine whether or not the waves were breaking. Even if this was physical data, with an observer to record breaking events, the exact definition of breaking is not widely agreed upon. The most common definition used is the process of converting potential and mechanical energy in a wave into other forms (heat, sound, light). In general, three different type of breaking criterion are considered [7]: 1) geometric, which usually relates to wave steepness or asymmetry, 2) kinematic, some form of crest acceleration or ratios between crest and phase speeds, and finally 3) energetic, when a wave passes a certain energy threshold.

For the purpose of this project, we will adhere to the criterion used by Professor Frederic Dias [7]. This involves calculating the ratio between the particle velocity at the peak, and the crest velocity. If this ratio exceeds a threshold value (usually either 0.85 or 0.7). We will also define a breaking period and length, which we generally take to be approximately 1/4 quarter the wave period and length respectively.

Below, we perform the above analysis on a JONSWAP spectra [9] under shoaling conditions. We use a criterion threshold of 0.85 and plot the surface elevation, local incidence angle, and the particle velocity of one of the breaking waves detected.

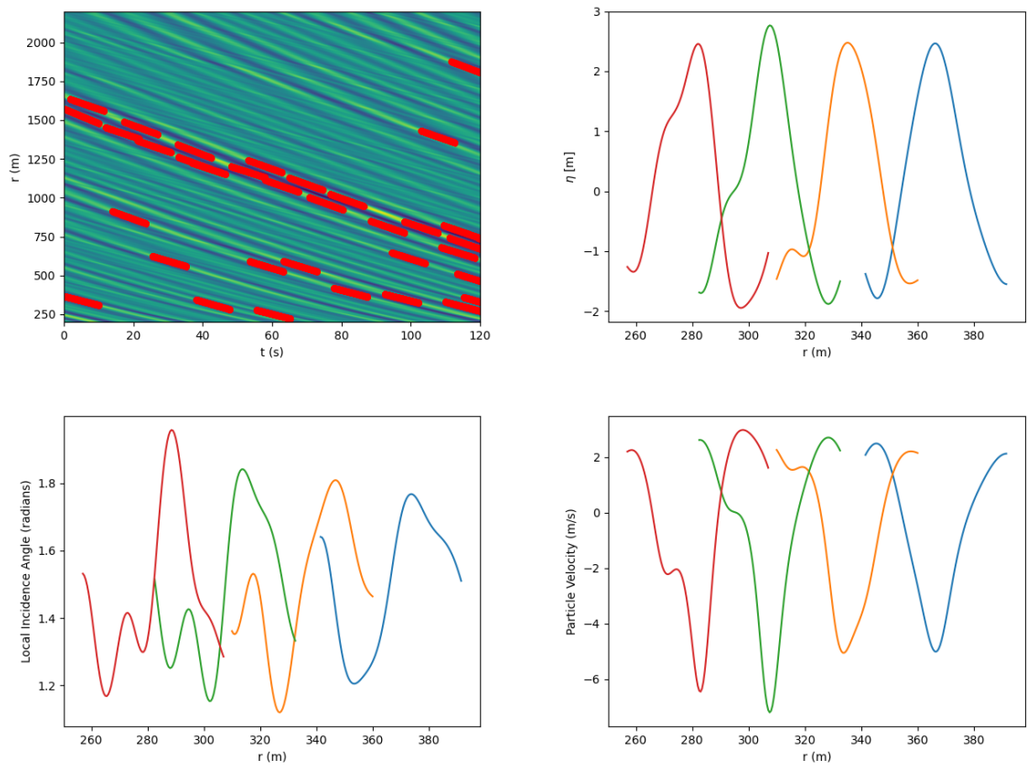

Figure 4: Top left: Red lines indicate breaking waves, overlaid on the physical surface elevation. Top right: Temporal evolution of the physical surface elevation of one of the breaking waves. Bottom left: Evolution of the local incidence angle of the same wave. Bottom right: Evolution of the particle velocity of the same wave.

4 Experimental Radar Data

In order to better develop the toolkit, we thought it best to work with some actual radar data alongside our simulations. The data used for the next two section were generously provided by Patricio A. Catalan and Merrick C. Haller [5], who performed their own analysis on the data. The data were recorded between the 10th of April and the 22nd of May 2008 at the US Army Corp of Engineers Field Research Facility, in Duke, NC. The radar data obtained used is of 1 spatial dimension, and 1 temporal dimension, and was recorded using RiverRad, an X-band (9.36 GHz), dual polarization (HH, VV) coherent radar, which was developed by the Applied Physics Lab at the University of Washington. The data were recorded along approximately 960 range lines, with the size of each spatial cell being approximately 7.5m. Data was collected along this line over 2 minutes, at which point the radar was rotated.

These data were then paired with data from a second remote sensing system [4], made up of three optical cameras from the ARGUS III observing station. This optical/video data was in the form of pixel intensity, and were collected at a sampling rate of 2 Hz for 31 min. These data were recorded over a rectangle, with coordinates spanning x = 60-600m and y = 500-1000m ($\delta x = 2$m, $\delta y = 5$m).

We were also provided with the bathymetry of the data collection area. While the time at which this bathymetry was measured was not the exact time at which the data collection were performed, previous measurements have shown that it is fairly consistent, with only minimal changes occurring in time.

As the exact range of the two sensors is not identical, for the purpose of this project we will only be interested in the overlapping area. While the provided RiverRad data were 1 dimensional, both the optical

data and the bathymetry were given over a 2D dimensional area. As such, both sets of data had to be interpolated along the radar line. For this we used cubic splines.

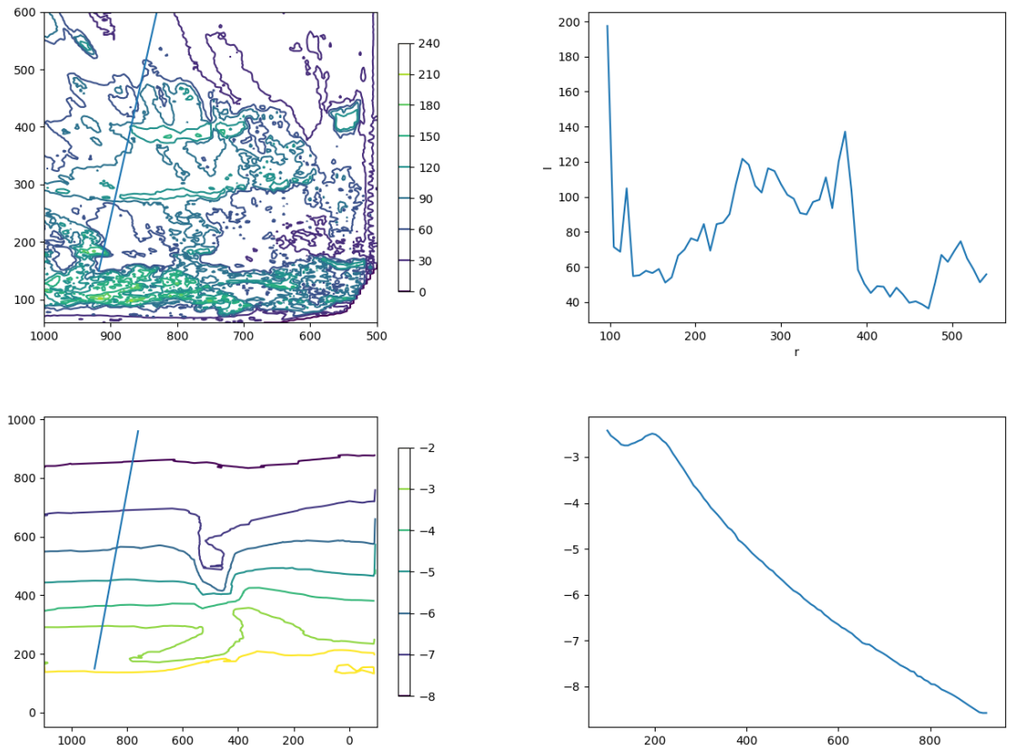

Figure 5: Top row: Contour map of the optical data, with the blue line indicating where the space in which the RiverRad data was calculated, and the interpolated intensity along this line respectively. Bottom row: Bathymetry of the area in which the experiment took place, with the blue line indicating where the space in which the RiverRad data were calculated, and the interpolated bathymetry along this line respectively.

5 Detection of Breaking using both Optical and Radar Data

It is well understood that both optical and radar data can be used when trying to discern breaking locations [1] [2]. However, both have their individual drawbacks. Large Doppler shifts are caused by both extremely steepened waves, and large brightness values can also be caused by remnant foam. As such, Patricio A. Catalan and Merrick C. Haller [5] sought to use a combination of both radar and optical data to decide whether breaking is occurring, or if the wave is simply steepened/remnant foam is obscuring the signal.

It should be noted that these thresholds are not found by derivation: they can vary with each data set, suggesting some type of dependence on environmental factors. For example, the position of the sun will effect the average intensity recorded by the optical cameras, and as such the threshold will need to be adjusted. It is noted that the Doppler threshold is generally found to be constant, as the yield of the RiverRad sensor is fixed. As well as this, the intensity seems to follow the relation $I^t = 2/3 * \hat{I}(x,t)_{\max}$, where $\hat{I}(x,t)_{\max}$ is the stpatial maximum over theb whole range over the total time. These observations were found by trial and error.

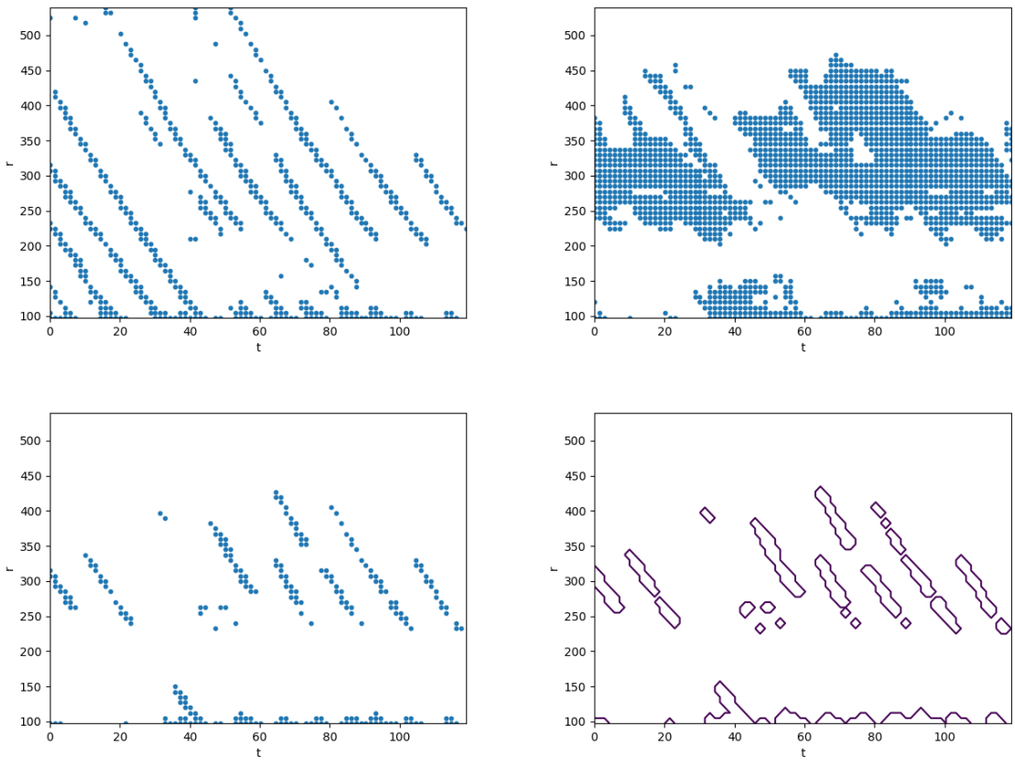

Figure 6: Top left: Breaking map using only the RiverRad data. Top right: Breaking map using only the optical data. Bottom left: Breaking map using the joint data method. Bottom right: Contour map of the breaking using the joint data method.

6 Radar Simulation

One of the governing imaging mechanisms by which a radar images a sea state can be assumed to be proportional to the local incidence angle. The local incidence angle is defined as the angle at which radio waves travel from the sea state to the radar antenna, with respect to the unit normal to the surface. This is easily pictured for 1D-waves, as shown below [8]:

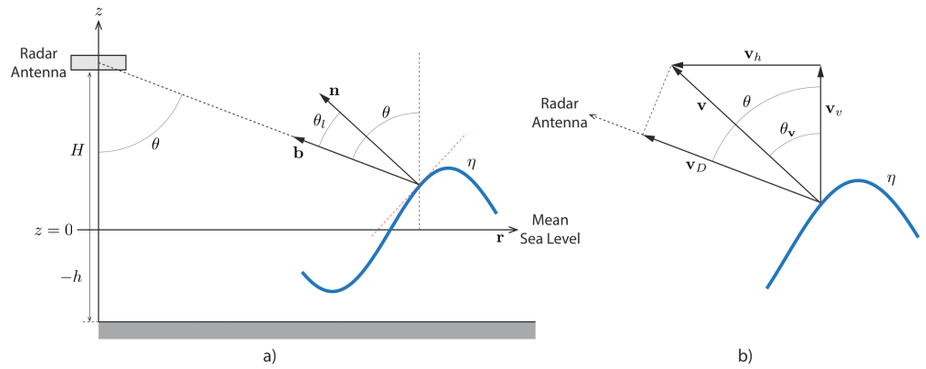

Figure 7: Geometry for calculating the local incidence angle (θ_l).

For 2D-waves, we can obtain this angle using the angle between two vectors, where we consider the vector pointing towards the radar, and the aforementioned normal to the sea surface. At any particular x, y, and η:

$$\cos\theta_L = \frac{x\frac{d\eta}{dx} + y\frac{d\eta}{dy} + (H-\eta)}{\sqrt{\left(\frac{d\eta}{dx}\right)^2 + \left(\frac{d\eta}{dx}\right)^2 + 1}\sqrt{x^2+y^2+(H-\eta)^2}}, \tag{9}$$

where all derivatives are evaluated locally. It can be assumed that the local incidence angle is proportional to the way in which a radar will read in a sea state. There are other uses however, one of which is the conversion of the local incidence angle into the physical sea surface (this is dealt with in more detail in the Appendix).

We will be using the JONSWAP spectra shoaling previously described to generate simulated sea surfaces, with which we can calculate the local incidence angle, which can then be used to simulate radar images.

We will replace the simple bathymetry with the interpolated one provided with the RiverRad data. We can therefore use the radar data from RiverRad to compare with our simulated radar data. Due to time constraints, we will simply be taking a first step in this modelling process, and will be adjusting the

parameters and scaling via trial and error. Given more time, one could search for the physical explanation to these equations. For this comparison, we used the horizontal polarised data, although both data sets present very similar features and characteristics.

First, we use the breaking detection method for simulated sea surfaces (the ratio criterion) to calculate the areas where breaking is occurring. In these sections, we replace the local incidence angle with a threshold value of our choosing, such that our altered local incidence angle $\theta_L^*(x,t)$ now is defined as:

$$\theta_L^*(x,t) = \begin{cases} \theta_L(x,t) & \text{No breaking detected} \\ \sigma_0 & \text{Breaking detected.} \end{cases}$$

This decision was based on the fact that for breaking waves, we generally saw a flat pulse of more or less constant height in the RiverRad data. Following this, we apply the equation:

$$\phi(x,t) = \left(20\left(\theta_L^*(x,t) - \bar{\theta}_L^*(t)\right)\right)^2 - 70, \tag{10}$$

where $\phi(x,t)$ is our simulated radar image, $\bar{\theta}_L^*(t)$ indicates the average value of $\theta_L^*(x,t)$ at a specific time. We began by shifting the data down so that they were centered roughly around -70 dB, as this was the typical value for non-breaking waves. Following this, we scaled the data so that it varied appropriately from wave to wave. We also ensured that the data held some form of continuity to it, and that waves that had not been detected to be breaking never produced a larger signal than those that were.

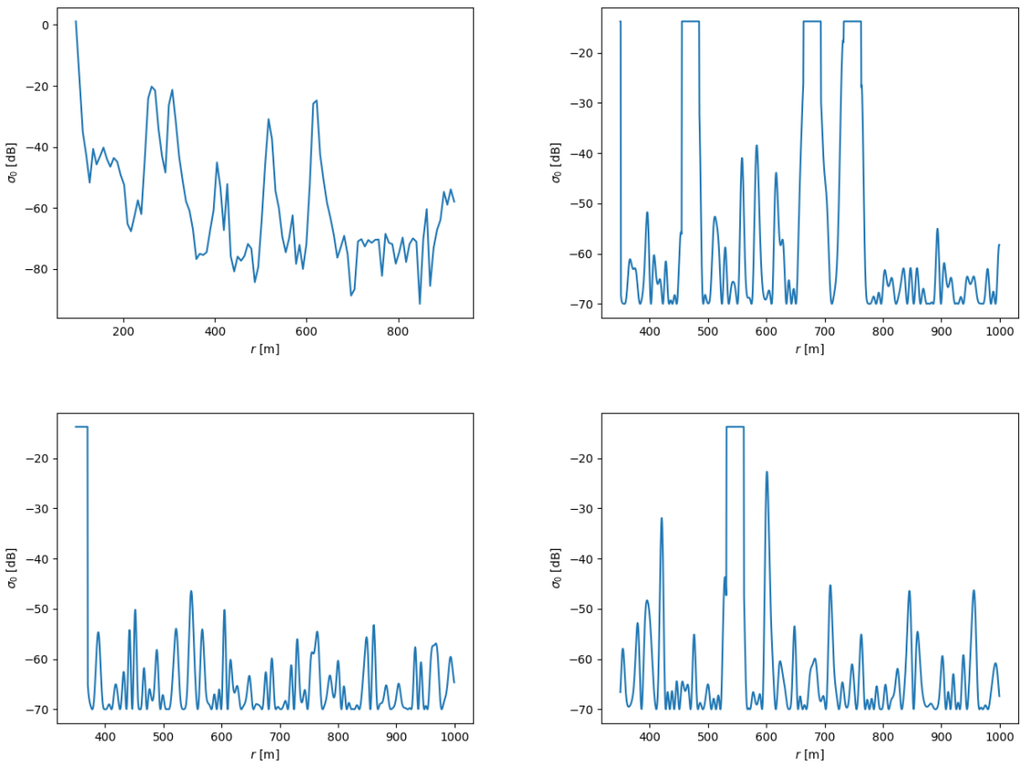

Figure 8: Top left: Slice of RiverRad data. The rest of the images are slices of our simulated radar data, at times showcasing different amounts of breaking.

7 Spatial Averaging

Along with building a simulated model for generating radar simulations, we also wanted to investigate at what spatial resolutions would we still have qualitatively the same image (i.e. when would we still be able to detect breaking). This understanding could be particularly useful in configuration of a radar, and in knowing what resolution might be required to acquire useful data.

The simulated model is better suited for this task, as we could create first a high resolution (spatially) simulation, and then slowly increase the scaling factor by which we average the cells, until we lost the characteristics on which the model was based. This was done by brute force, slowly increasing the averaging factor and inspecting the image by eye. We then applied this same averaging to the observed data, to check if our "critical point" in which one loses the shape of the data is consistent between the observed set and our simulated set.

For the run shown in the figure below, we used a breaking length of 15m. We plot the values for dx $= 15, 25, 30, 35$ metres. We also plot the physical surface elevation at this time for comparison. We can see that at first we lose the shape of the smaller waves, however the signature of breaking is still present.

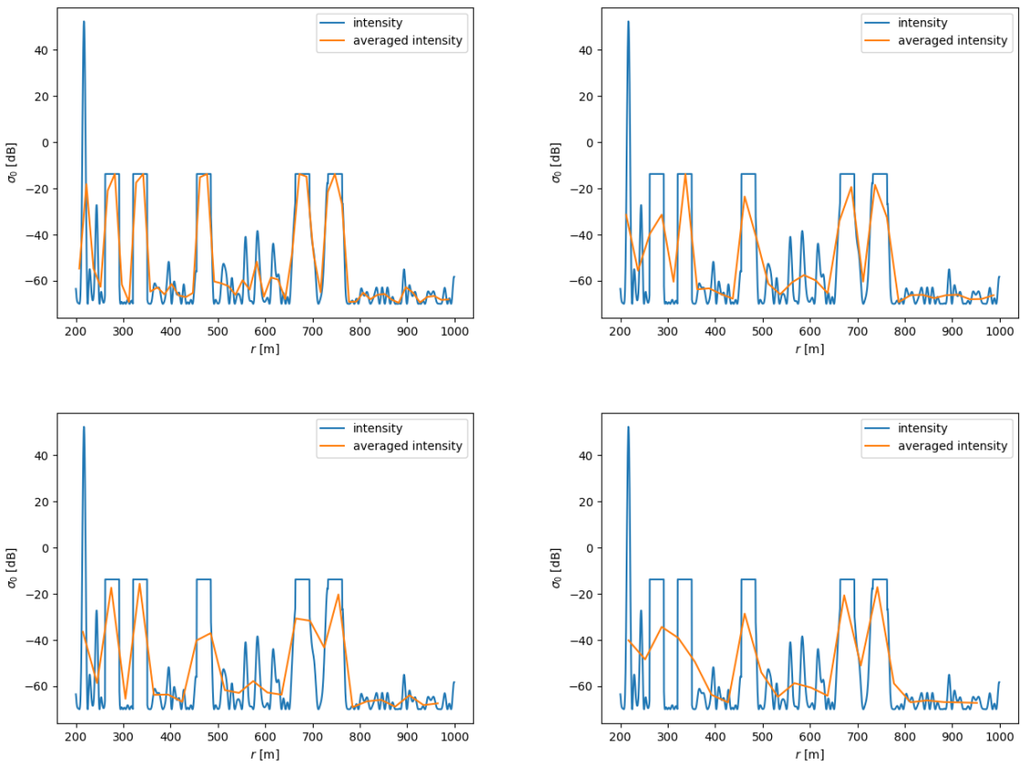

Figure 9: From top to bottom, left to right: Plots showcasing our averaged data versus the original data, increasing in coarseness.

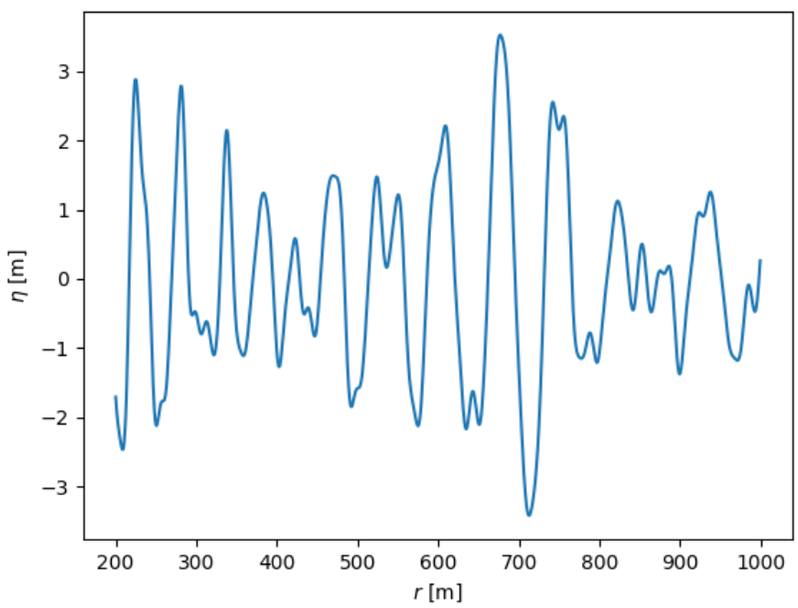

Figure 10: Physical surface elevation at the time used for the plots above for comparison.

This was then repeated for RiverRad data, although due to the "coarseness" of this data we could only inspect the effects of averaging over two and three cells before all of the original qualities of the data were lost.

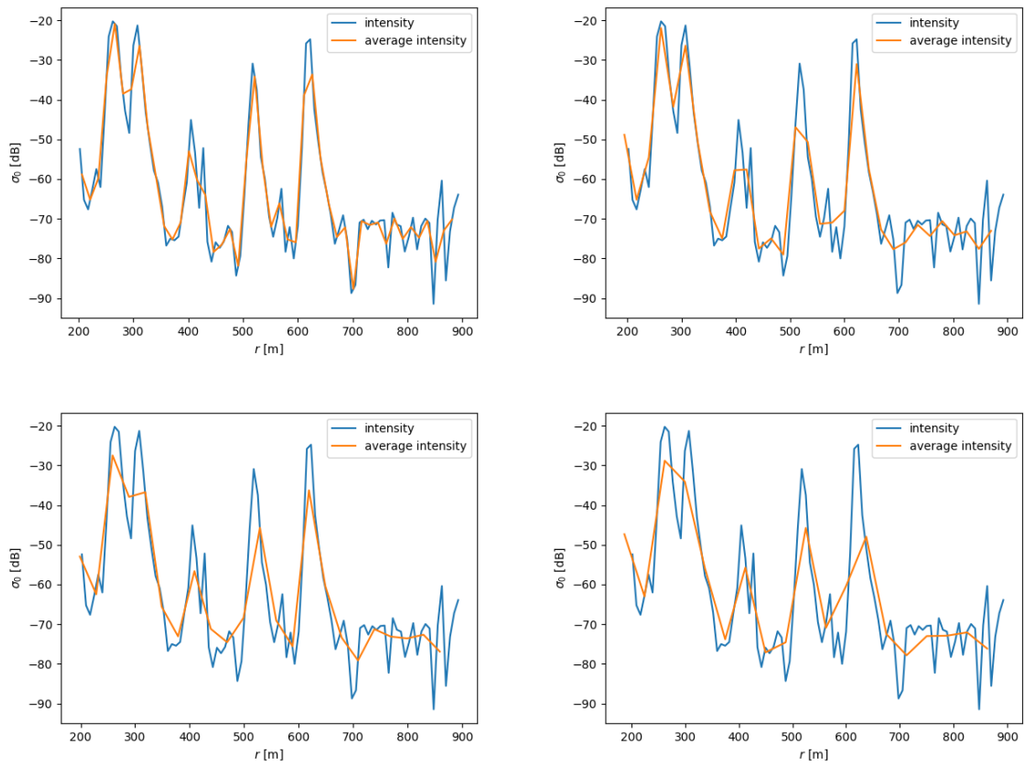

Figure 11: From top to bottom, left to right: Plots showcasing the averaged RiverRad data versus the original data, increasing in coarseness.

Finally, we sought out a relationship between the breaking length and the resolution at which the data was still meaningful. We considered several different values of breaking length, and decreased the resolution until we lost the breaking events. This was defined as peaks falling below the threshold used previously so that the event would be completely lost, or that two separate events would "merge" into one. This yielded a ratio of breaking length to grid step size of:

$$\frac{\text{Breaking Length}}{\text{Resolution}} \approx 1.02. \tag{11}$$

This is in line with previously cited values that for breaking signatures to be properly detected, you must have that the entire radar cell is entirely occupied by the breaking wave [10].

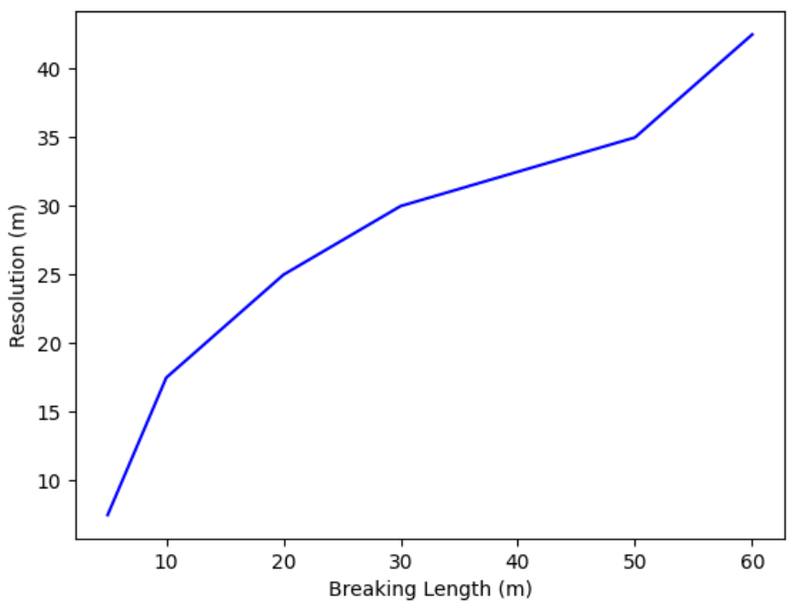

Figure 12: Breaking length vs. the maximum resolution before the qualities of the simulated data were lost.

The criterion used to obtain the above data was mostly done by eye: for each breaking length, we would increase the coarseness of the data by increments of 2.5m, until either non-breaking peaks had larger signatures than breaking ones, or breaking peaks merged together.

8 Discussion

With regards to the observed data, it is evident from our investigation into the relationship between breaking length and resolution that if our radar images over a grid that is not fine enough, we may miss smaller-scale breaking events. There are also further limitations in that there is no "hard truth" to compare against: the exact physical surface elevation is not available, and while the optical data may help indicate that we are correctly identifying wave breaking it cannot be certain that we catch all events, and also that all the waves that we determine to be breaking actually are.

These issues could be rectified with more data: It will become more and more clear whether or not we are properly identifying wave breaking events with more data sets, as well as ensuring that the method generalises well for different sea states with different environmental conditions.

With regards to the simulated data, one potential issue is that the equations for the shoaling conditions are derived from linear theory, and so we could be missing nonlinear interactions that are known to lead to extreme wave heights (and inevitably wave breaking). Our equation for generating radar data from the local incidence surface is also somewhat arbitrary, and was found by inspection.

It is also important to note some of the current differences between the RiverRad data and our simulated data. Firstly, there appears to be some form of non-linearity in our model at lower values for non-breaking waves (around -65dB). This is likely due to the fact that we apply a square to the local incidence angle, which will reflect the negative values for the local incidence angle. Our model does also has large spikes for peaks that come too close to the radar: this is due to the formulation of the local incidence angle, and our choice of radar height. Some type of filter could be applied later to help smooth this out (similar to what is described in the Appendix).

This simulated model however should be seen as a first iteration of the model, and is meant to be improved upon. The initial simulated surface can easily be swapped out for other, more accurate/high level simulations. As well as this, the equations we derived for generating radar data are a first step: given more time, we would like to derive these relations. However, these equations will hopefully assist in guiding this derivation.

9 Conclusion

We built a simple radar imaging model for wave breaking with shoaling conditions. This model first generates sea states based off of a JONSWAP spectra with shoaling conditions, and calculating the relevant local incidence angle. This was then compared with observed data, provided by the RiverRad experiment, and was scaled and shifted to obtain the relevant features and qualities. We then used this model to investigate the relationship between the length of breaking, and the resolution required to properly capture the breaking event. It was found that the ratio between these two features is approximately 1.02, which aligns well with previous conclusions that wave breaking can only be detected if it covers the entire cell [10].

10 Acknowledgements

We would first like to thank the SFI CRT in Foundations of Data Science for funding this summer undergraduate research project, as this research project would not have been possible otherwise. We would also like to thank Patrico A. Catalán and Merrick C. Haller for kindly allowing us to use their data, and for their input through the project. Finally, we would like to thank Frederic Dias for facilitating this project, and Susanne Støle-Hentschel for her expertise, guidance, and help throughout the course of this project.

References

[1] R. Holman and J. Stanley (2007), The history and technical capabilities of ARGUS. (Coastal Engineering Vol. 54)

[2] Guillermo M. Díaz Méndez, Merrick C. Haller, Britt Raubenheimer, Steve Elgaar, David A. Honegger (2014), Radar Remote Sensing Estimates of Waves and Wave Forcing at a Tidal Inlet. (Journal of Atmospheric and Oceanic Technology Vol. 32)

[3] Pavel V. Chernyshov (2020), Remote Sensing of the Nearshore Region. (PhD thesis Tel Aviv University).

[4] Patrico A. Catalán, Merrick C. Haller, Robert A. Holman, William J. Plant (2011), Optical and Microwave Detection of Wave Breaking in the Surf Zone. (IEEE Transactions on Geoscience and Remote Sensing Vol. 49).

[5] Patrico A. Catalán, Merrick C. Haller, William J. Plant (2014), Microwave backscattering from surf zone waves. (Journal of Geophysical Research: Oceans).

[6] José C. Nieto Borge, Germán Rodríguez Rodríguez, Katrin Hessner, Paloma Izquierdo González (2003), Inversion of Marine Radar Images for Surface Wave Analysis. (Journal of Atmospheric and Oceanic Technology Vol. 21).

[7] X. Barthelemy, M. L. Banner, W. L. Peirson, F. Fedele, M. Allis, F. Dias (2018), On a unified breaking onset threshold for gravity waves in deep and intermediate depth water. (Journal Fluid Mechanics Vol. 841).

[8] Susanne Støle-Hentschel, Jörg Seemn, José Carlos Nieto Borge, Karsten Trulsen (2018), Consisteny between Sea Surface Reconstructions from Nautical X-Band Radar Doppler and Amplitude Measurements. (Journal of Atmospheric and Oceanic Technology Vol. 35)

[9] Hasselmann K., T.P. Barnett, E. Bouws, H. Carlson, D.E. Cartwright, K. Enke, J.A. Ewing, H. Gienapp, D.E. Hasselmann, P. Kruseman, A. Meerburg, P. Mller, D.J. Olbers, K. Richter, W. Sell, and H. Walden, (1973), Measurements of wind-wave growth and swell decay during the Joint North Sea Wave Project (JONSWAP) Ergnzungsheft zur Deutschen Hydrographischen Zeitschrift Reihe, A(8) (Nr. 12)

[10] B. L. Lewis, I. D. Olin (1980), Experimental study and theoretical model of high-resolution radar backscatter from the sea. (Radio Science Vol. 15)

A Appendix

Given a radar image, the steps taken to convert this to a physical surface elevation are as follows [6]:

1. Collect the stack of images (i.e. a cuboid of data, with each slice being the sea state at a given time).
2. Apply the 3D fast Fourier transform.
3. Apply a high pass (HP) filter.
4. Apply a dispersions filter.
5. Apply a modulation transfer function (MTF).
6. Apply the 3d inverse fast Fourier transform to recover the physical surface elevation.

For the purpose of this project, we will be working with simulated sea states (either sinusoidal or JONSWAP spectra, under shoaling conditions for varying bathymetries), and as such no noise is present. This means that we leave out the application of the dispersions filter.

We begin with our sea state as presented below, with a radar placed 20m above the mean wave height.

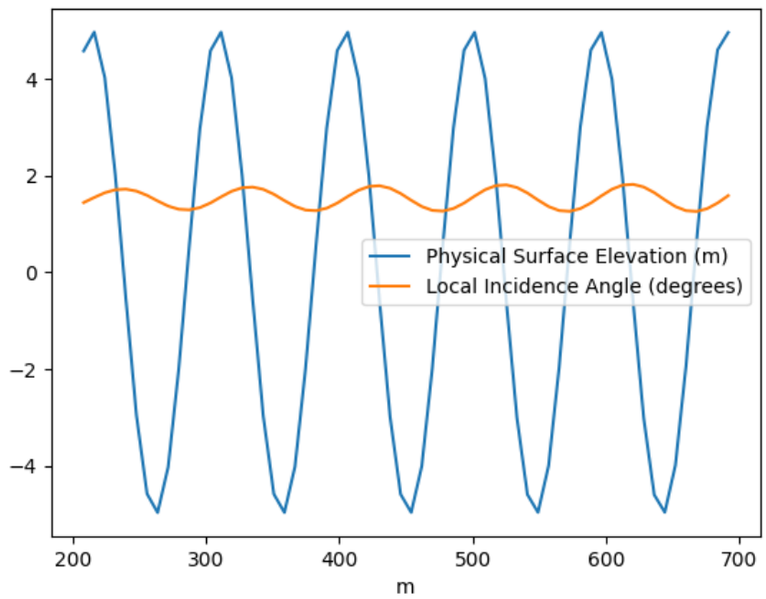

Figure 13: Slice of the physical surface elevation and local incidence angle for a sinusoidal wave.

Figure 14: 3D images of the physical surface elevation and local incidence angle, respectively.

The sea state we are considering is 200m off shore, on a 500m by 500m grid. We next apply the 3D fast Fourier transform on the local incidence surface:

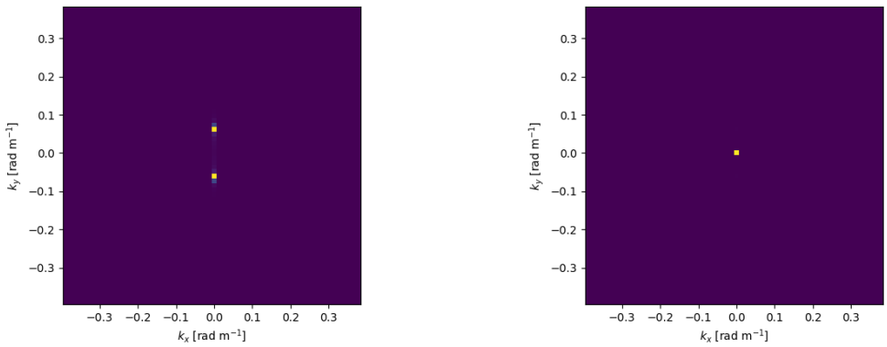

Figure 15: Fourier transform of the physical surface elevation and local incidence angle, respectively.

Next we apply the HP filter. We can convert this back to the physical domain temporarily to see what is obtained without an MTF. We see that the physical height is reduced by a factor of 10, with some slight modulations.

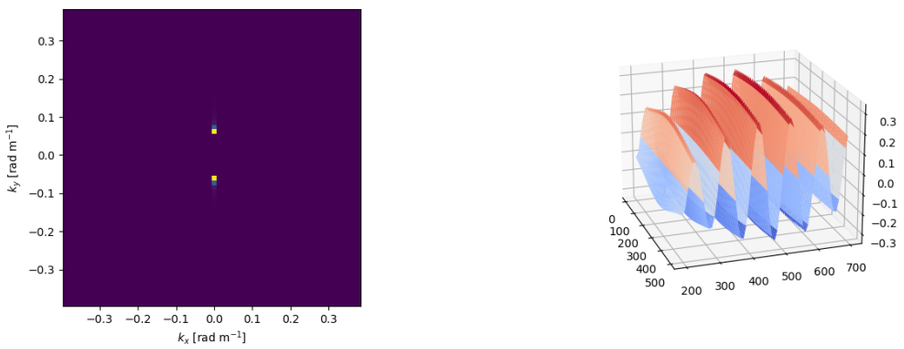

Figure 16: Fourier transform of the local incidence angle after applying the HP, as well as the function in physical space after applying the inverse Fourier transform.

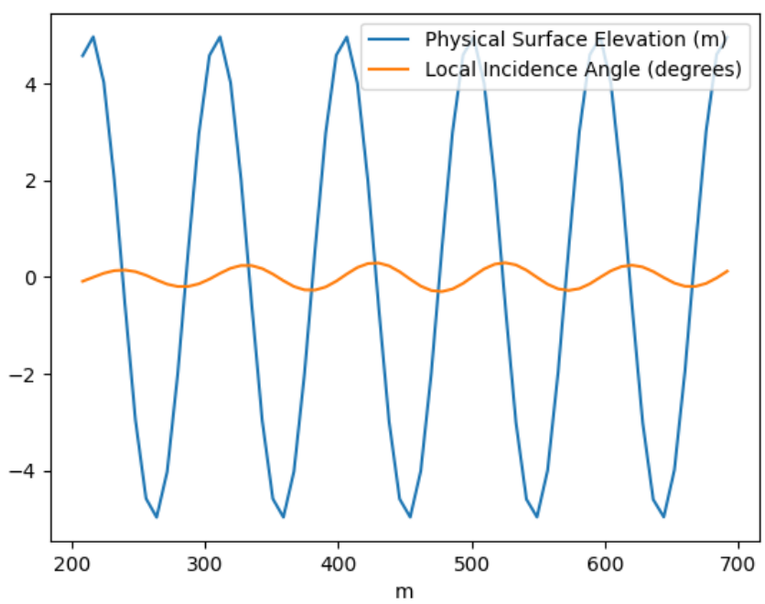

Figure 17: Slice comparing the physical surface elevation to the local incidence angle after applying the HP.

Finally, we again consider the spectral form following the HP filter, and now apply the MTF. Reverting to the physical domain, we see that the wave height is now much more in-line with our original sea state, with the shape closely mimicking it.

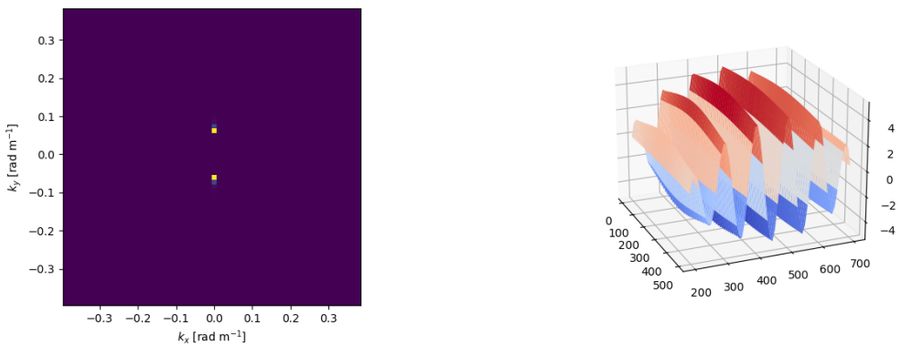

Figure 18: Fourier transform of the local incidence angle after applying the MTF, as well as the function in physical space after applying the inverse Fourier transform.

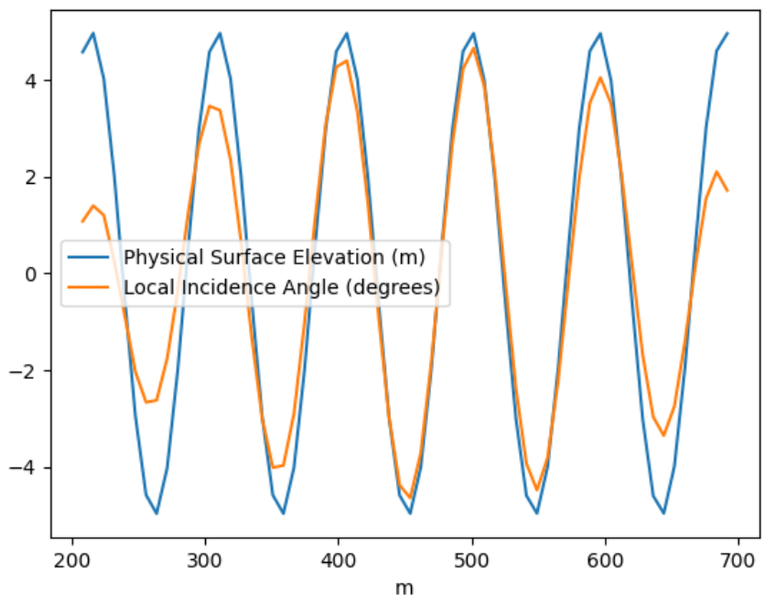

Figure 19: Slice comparing the physical surface elevation to the local incidence angle after applying the HP. One can see that this has mostly recovered the physical surface elevation (apart from issues near the boundaries of the grid).